POLYMERS WITH TRIAZENE UNITS IN THE MAIN CHAIN

Application for Laser-Lithography

Oskar Nuyken,[1] Jürgen Stebani,[1] Alexander Wokaun,[2] and Thomas Lippert[2]

[1] Lehrstuhl für Makromolekulare Stoffe
TU München
Lichtenbergstr. 4
D-85747 Garching
Germany
[2] ETH Zürich and Paul-Scherrer-Institut
CH-5232 Villigen
Switzerland

ABSTRACT

Several monomeric and polymeric triazenes have been synthesized and characterized by common methods such as ^{1}H NMR-, IR-, Raman-, UV-spectroscopy, DSC, and GPC. Their thermolysis, photosensitivity, and the effect of H_3O^+ on their stability have been studied in detail, since those characteristics are very important for an application of these compounds in microlithography.

In laser ablation experiments, polymers containing triazene units in the main chain (**TP1 - TP9**) exhibited several advantages over systems in which common polymers (e.g. PMMA) are doped with low molecular triazenes (**T1 - T14**), especially the fact that their ablation craters have clean contours and sharp edges is of great interest for this type of microstructering.

1. INTRODUCTION

"Triazenes" (R_1-N=N-N(R_2)(R_3)) are rather "old" compounds from the organic chemists viewpoint. It was as early as 1862 that Griess described a suitable way for the synthesis of 1,3-diphenyltriazene [1]. Since one could not find any application for triazenes at that time, these compounds have been ignored for many decades. Moreover, they have been considered an undesired sideproduct in the azo-dye synthesis.

Unsubstituted triazenes are unstable under normal conditions. Substituted triazenes, however, can be rather thermally stable. In newer time, some attention was paid to substituted

Macromolecular Engineering, Edited by M.K. Mishra et al.
Plenum Press, New York, 1995

triazenes, especially to 1-aryl-3,3-dialkyl-triazenes, which were synthesized for the first time in 1875 [2] because some of them show activity as insecticides and anti-tumor properties [3]. This is also the main reason for more than 1200 references on triazenes in the last 20 years.

A rather modern aspect, and the main reason for our interest in triazenes, is their potential in the information storage technology, mainly due to their high photosensitivity [4,5]. Therefore we have studied the ground state and excited state properties of selected 1-aryl-3,3-dialkyl-triazenes but also of polymers containing triazene groups as part of the main chain in some detail.

2. SYNTHESIS AND GROUND STATE PROPERTIES OF TRIAZENES

The most suitable route for the synthesis of triazenes is given in the following scheme:

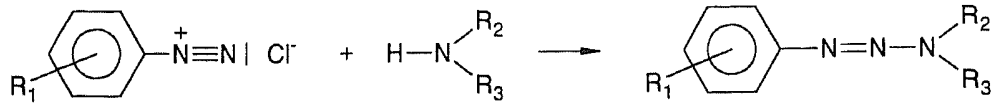

Triazenes are photosensitive, thermosensitive, and sensitive against protons. Furthermore, their stability is strongly influenced by their substitution pattern. Thermolysis and photolysis yield radicals as intermediates, meanwhile the retrosynthetic route to diazonium ions and amines is forced by protons.

From X-ray it is known that the most stable isomer has a trans- conformation at the N=N-bond [6].

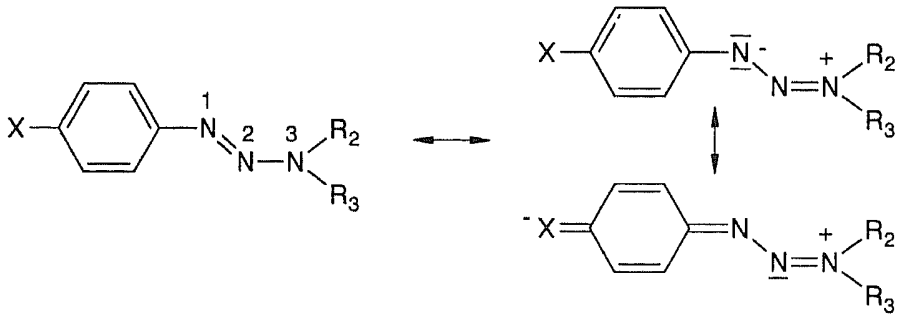

The 1,3-dipolar structures become increasingly important when the aromat is substituted with electron acceptor groups such as NO_2 or CN. In this case the rotation barrier around the N^2-N^3 bond increases [7].

To support the existence of this rotation barrier we carried out ^{1}H NMR experiments for selected triazenes in d_4-methanol at different temperatures. As shown in Table 1, the highest coalescence temperatures were determined for compounds with electron withdrawing substituents on the aromatic ring(**T1,T2**). A typical NMR pattern in these experiments is given in Fig.1:

The Hammett-plot (Fig.2) of the rate constants of the rotation around the N^2-N^3 bond at 273 K, obtained from the NMR experiments, results in $\rho = -1.95 \pm 0.21$ which is in good agreement with literature values [8,9]. The negative value is a clear indication for a rotation barrier due to the π -overlapping of azo and amine orbitals. Furthermore it supports the postulated 1,3-dipolar structure.

Table 1. Coalescence temperature for model triazenes of the structure R_1-Ph-N=N-N(R_2)(R_3) ($R_2 = R_3 = C_2H_5$)

Compound	R_1	T (K)
T1	4-NO_2	308
T2	4-CN	302
T3	4-COOH	283
T5	H	255
T7	4-OCH_3	238
T9	3,5-di(COOH)	280
T11	3-COOH	284
T13	3-COOH*	274
T14	3-COOH**	285

* $R_{2,3}$ = n-propyl; ** $R_{2,3}$ = isopropyl

3. THERMOANALYSIS OF TRIAZENES

From thermolysis data one can get information about the thermostability, which is important not only from the academic view point but also from the view point of safety and application. Therefore selected triazenes have been studied by DSC (differential scanning calorimetry) to determine the decomposition temperatures and the decomposition rate constants [compare ref. 10].

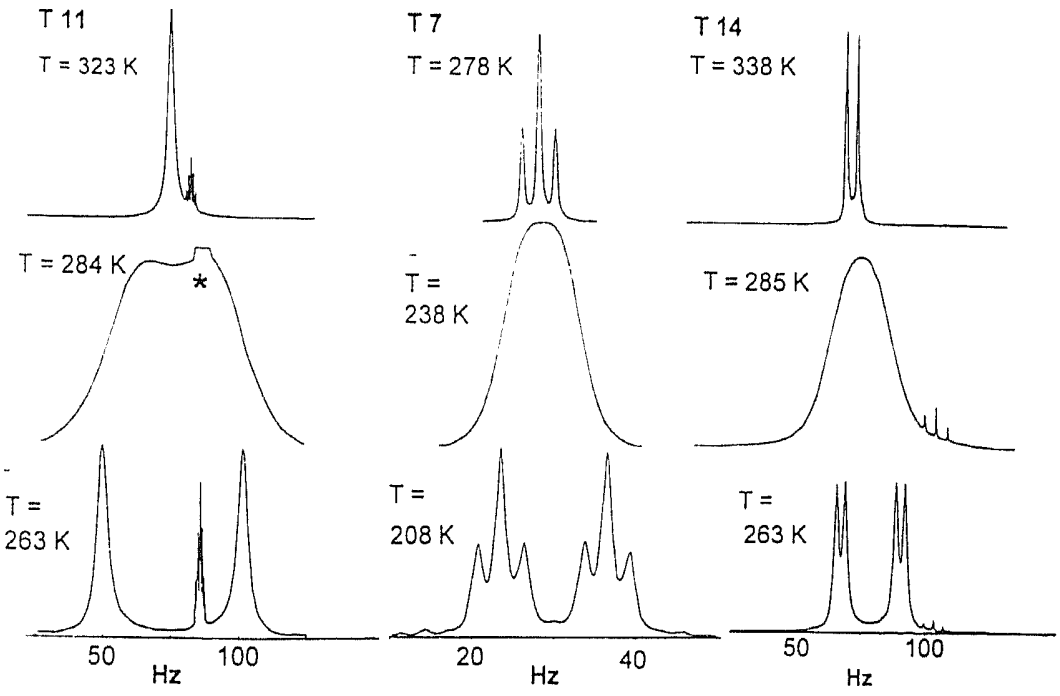

Figure 1. ^{1}H NMR of methyl protons (**T11, T7**) and methin protons (**T14**) of triazenes at different temperatures.

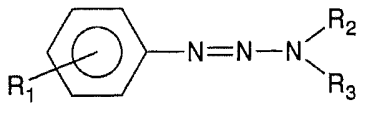

abbrev.	R_1	R_2	R_3
T11	3-COOH	C_2H_5	C_2H_5
T7	4-OCH_3	C_2H_5	C_2H_5
T14	3-COOH	C_2H_5	$CH(CH_3)_2$

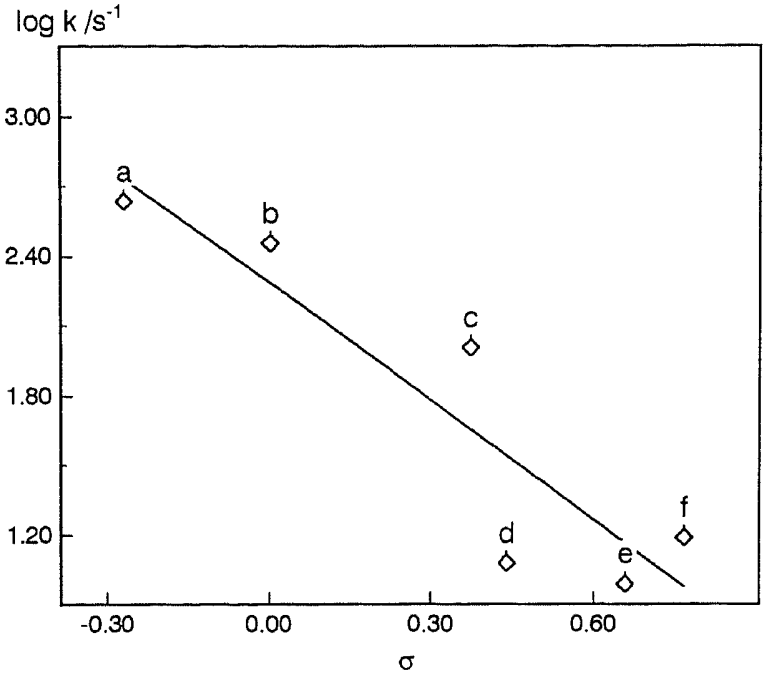

Figure 2. Hammett-plot for the rate constants for the hindered rotation around N^2-N^3 bond in different triazenes at 273 K; a) **T7**, b) **T5**, c) **T12**, d) **T3**, e) **T2**, f) **T1**.

A typical result (arrhenius plot of the rate constants at different temperatures, determined by DSC) for triazenes is shown in Fig.3 for **T9**.

The thermolysis experiments quite clearly showed, that triazenes having electron withdrawing substituents in para-position of the aromatic ring stabilize the compound. Some of the models do not decompose at T<200°.

The thermolysis of triazenes has been studied several times [11-13]. Aromatic triazenes (1,3-diaryltriazenes) decompose thermally via radicalic intermediates under rapture of the N^2-N^3-bond.

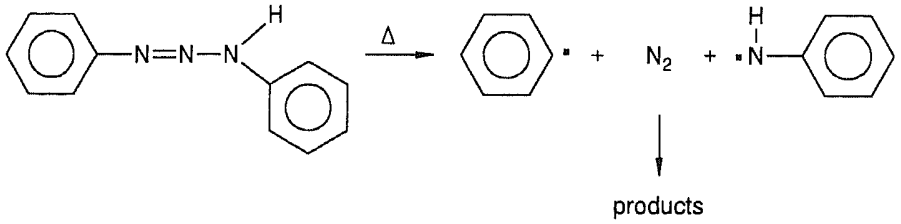

The products depend strongly on the solvent used, e.g. decomposition in benzene yields diaryls, decomposition in alcohols yields ethers [14]. The intermediate radicals were

Table 2. Decomposition temperatures T_{max} and E_a for different triazenes (measured by DSC in bulk), structures R_1-Ph-N=N-N(R_2)(R_3)

Compound	R_1	R_2, R_3	T_{max} (°C)	E_a (kJmol^{-1})
T3	4-COOH	di-C_2H_5	148	242
T9	3,5-di(COOH)	di-C_2H_5	151	282
T11	3-COOH	di-C_2H_5	113	282
T13	3-COOH	di-n-propyl	128	221
T14	3-COOH	di-isopropyl	136	—*
T15	4-OCH_3	CH_3, $(CH_2)_{17}CH_3$	270	—*
T16	4-CN	CH_3, $(CH_2)_{17}CH_3$	308	—*

* not determined

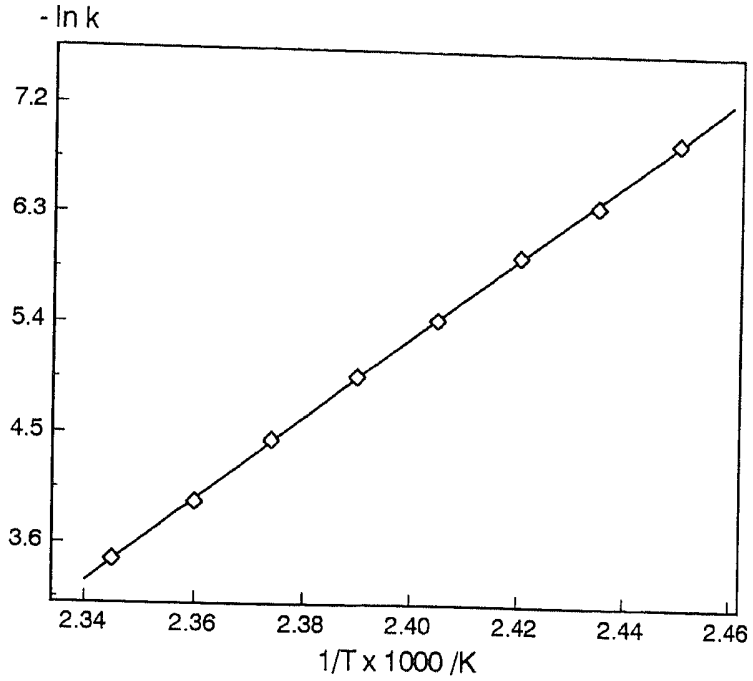

Figure 3. Arrhenius-plot of the decomposition of **T9** in bulk, measured by DSC.

found to be able to initiate a free radical polymerization, e.g. of butadiene, a copolymerization of acrylonitrile with vinylpyridine, and others [11-13, 15].

An interesting observation was that addition of acids reduce the decomposition temperatures of triazenes [16]. Therefore we found it necessary to study the effect of protons on the decomposition of triazenes in some detail.

4. PROTOLYSIS OF TRIAZENES

It is known from earlier work that triazenes decompose in the presence of acids. Di- and trialkyltriazenes [17], 3-alkyl-1-aryltriazenes [18,19], and 3-alkyl-1,3-diaryltriazenes [20,21] are studied in detail. Surprisingly little is known, however, for the protolysis of 1-aryl-3,3-dialkyltriazene [22-24].

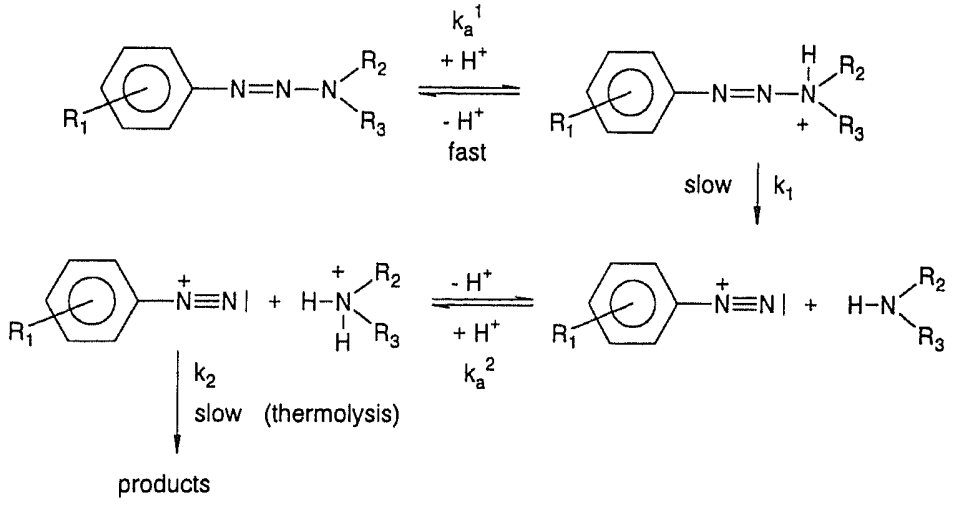

Typical experiments were carried out in buffer -methanol mixtures in the presence of a 5 fold concentration of NaCl compared to the triazene ($8 \cdot 10^{-5}$ mol l^{-1}). The decrease of

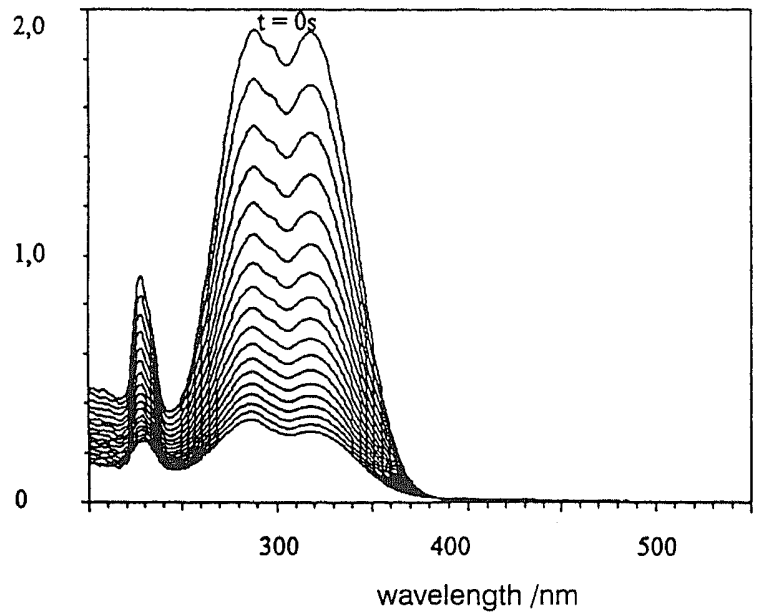

Figure 4. Protolysis of R_1-Ph-N=N-N$(C_2H_5)_2$ (R_1 = Cl), followed by UV-spectroscopy, pH = 4.7, RT, intervals: 60 min.

triazene concentration with time was measured at room temperature in different buffer solutions. A characteristic example for a protolysis experiment followed by UV-measurements is presented in Fig 4.

The effective rate constants as a function of pH values results in straight lines for all triazenes investigated in this work (Fig. 5). Meanwhile **T8** (R_1 = 4-N$(CH_3)_2$) decomposes already at pH = 10 with a half life time of only 100s, **T1** (R_1 = 4-NO_2) is very resistant against the retrosynthetic decomposition.

From the decomposition scheme for the protolysis of triazenes results (E1):

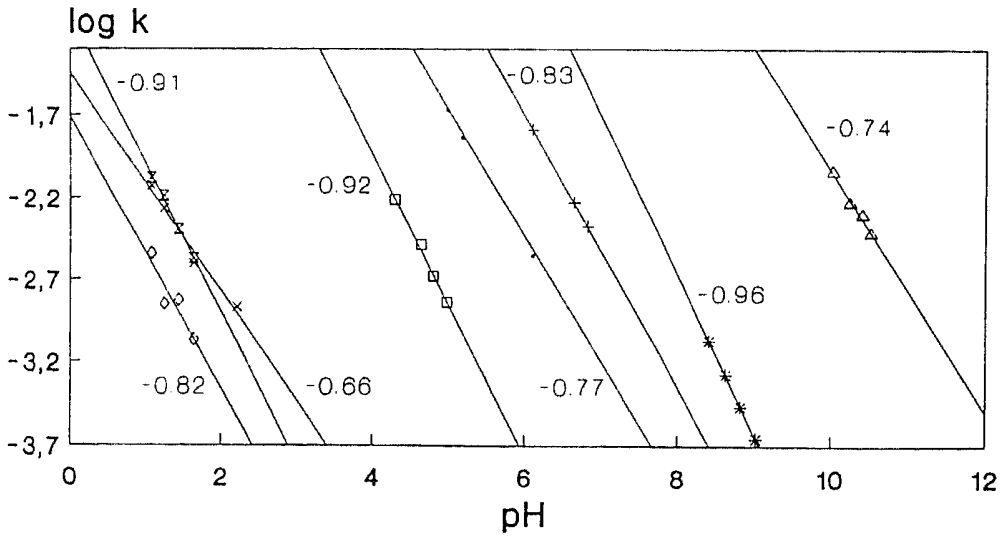

Figure 5. Dependence of the effective first order rate constants of triazene decomposition on solution pH. For each curve the slope of the corresponding linear regression is included in the figure. Structures according to Table 1, R_1=H (■), CH_3 (+), OCH_3 (✳), Cl (□), CN (x), NO_2 (⊖), N$(CH_3)_2$ (Δ), m-NO_2 (⧖).

$$k_a^l = \frac{[TH^+]}{[T]\,[H_3O^+]} \tag{E1}$$

Ka^l equilibrium constant of protonation
$[T]$ concentration of the triazene in equilibrium
$[TH^+]$ concentration of the protonated triazene in equilibrium

If unimolecular decomposition of $[TH^+]$ is rate determined then (E2) is valid:

$$-\frac{d[T]}{dt} = k_1\,[TH^+] = k_1\,k_a^l\,[T]\,[H_3O^+] \tag{E2}$$

In this case the effective rate constant depends on H_3O^+ concentration and the decomposition reaction has the characteristics of a specific acid catalysis.

Systematic variation of the buffer concentration and of the buffer type (pH = 2 for glycine or citrate buffer) shows that "specific acid catalysis" is a suitable description for the protolysis of triazene, since the reaction depends not on the chemical nature of the buffer but on the actual H_3O^+ concentration only. This view is also supported by deuterolysis: D_2O was used for protolysis instead of H_2O. The isotope effect (differences in the rate constants) was determined to be $k_H/k_D = 0.432$. Since D_3O^+ is a stronger acid than H_3O^+ the reaction is faster in D_2O than in H_2O.

As already mentioned above, the protolytic stability is dramatically influenced by the substituents at the aromatic ring of the triazenes. A comparison of the rate constants for the decomposition of triazenes at pH=7 is given in Table 3. The Hammett-plot for these results (Fig. 6) is a straight line, resulting in $\rho = -4.70$ which is quite similar to a value given in the literature for 1-aryl-3,3-dimethyltriazene ($\rho = -4.03$) [24].

The linear dependency of the triazene decomposition on the H_3O^+ concentration opens the chance to control the rate by variation of the pH-value. An additional possibility to produce protons is given by irradiation of photo acids e.g. sulfonium salts. Those investigations are in progress.

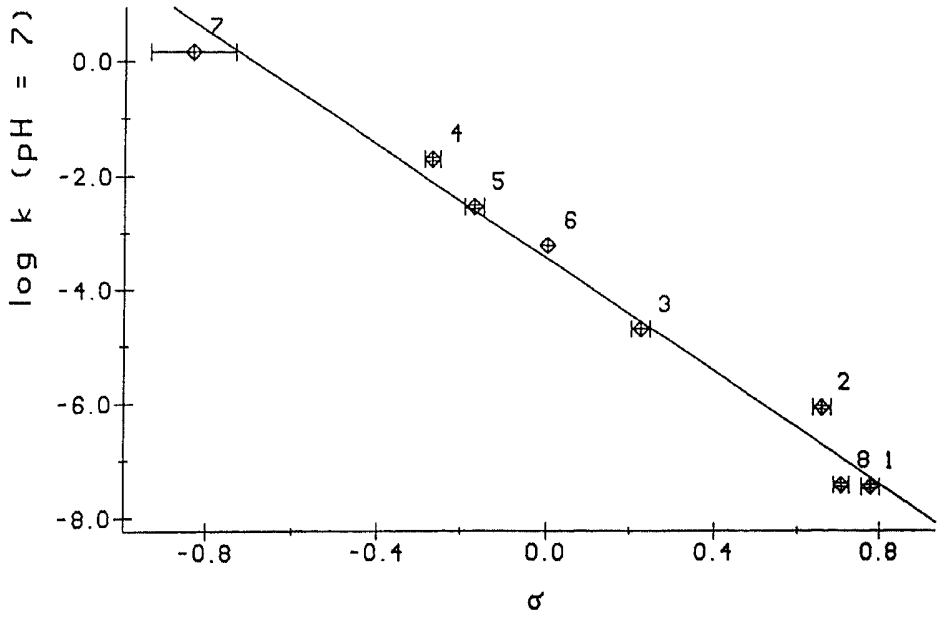

Figure 6. Hammett-plot for the protolysis of triazenes **T1 - T9** at room temperature, pH=7; 1=**T1**, 2=**T2**, 3=**T4**, 4=**T7**, 5=**T6**, 6=**T5**, 7=**T8**, 8=**T12**.

Table 3. Extrapolated rate constants $k_{exp.}$ at pH = 7 for different triazenes R_1-Ph-N=N-N$(C_2H_5)_2$

Triazene	Substituents	- log $k_{exp.}$	$t_{1/2}$
T1	4-NO_2	- 7.470	39 years
T12	3-NO_2	- 7.430	36 years
T2	4-CN	- 6.068	2 years
T4	4-Cl	- 4.676	23 days
T10	3-OCH_3	- 3.629	2 days
T5	H	- 3.197	18 h
T6	4-CH_3	- 2.522	4 h
T7	4-OCH_3	- 1.697	35 min
T8	4-$N(CH_3)_2$	0.170	28 s

5. PHOTOLYSIS OF TRIAZENES

Among the 1200 papers published on triazene chemistry in recent years there are only few dealing with the photochemistry of these compounds and those mostly are related to 1,3-diaryltriazenes and their application as doping material for laser ablation of polymethylmethacrylate [25-27].

Irradiation of triazenes with UV-light in general yields radicals and nitrogen:

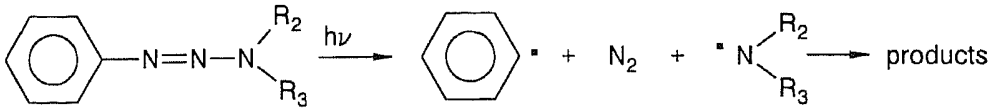

The radical intermediates have been detected by ESR-spectroscopy [28]. A typical photolysis experiment is shown in Fig. 7.

The observed isosbestic points (1-3) are a clear indication for a well-defined decomposition mechanism, which is suitable described by a first order kinetics [29,30]. The uniformity of the decomposition is strongly supported by evaluation in Mauser plots according to (E3) (Fig.9) [31-34] in which straight lines were observed for most triazenes.

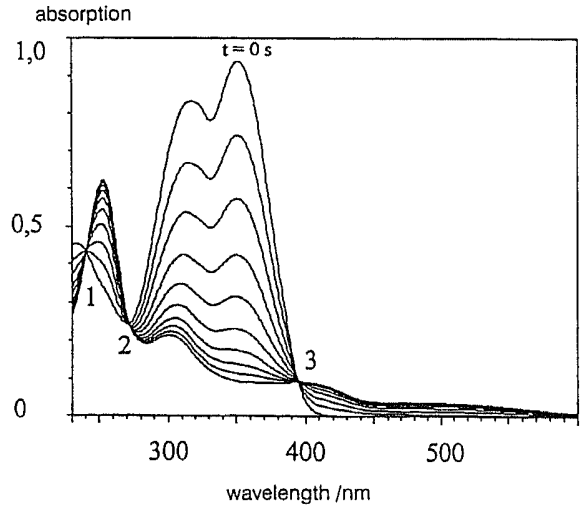

Figure 7. Photolysis of **T7** in THF, RT, followed by UV-spectroscopy, 0.2s intervalls; lamp: Xe-high pressure.

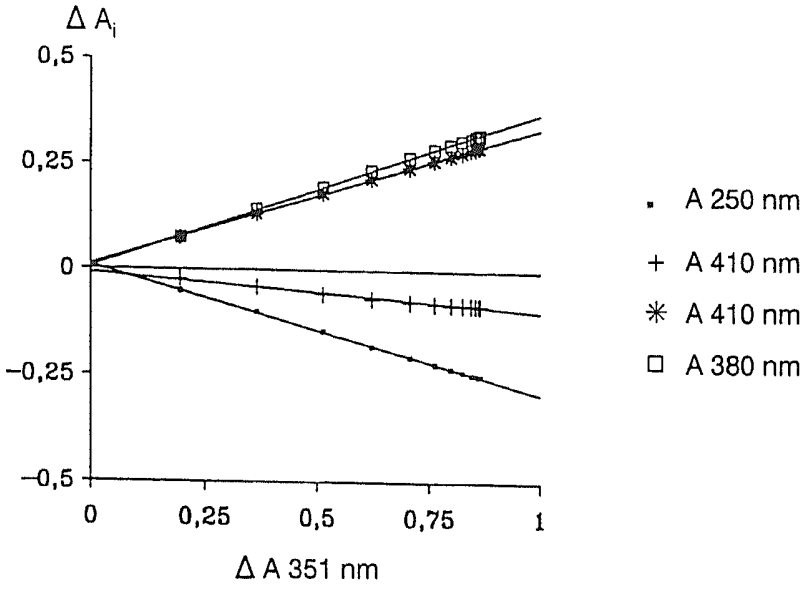

Figure 8. Mauser plot for the photolysis of 4-N$(CH_3)_2$-Ph-N=N-N-$(C_2H_5)_2$ (**T8**) in THF at room temperature for four different wavelengths; lamp: Xe-high pressure.

$$\Delta A_{i_t} = f(\Delta A_t) \tag{E3}$$

ΔA_{i_t} = difference between absorption at t = 0 (A_0) and absorption at t=t for a certain wavelength

ΔA_t = difference between A_0 and A_t for a reference wavelength.

Since the uniformity of the photolysis is confirmed one can determine the actual rate constants. A Hammett-plot of these rate constants results in a straight line, from which it was possible to determine ρ = -2,13. The advantage of the availability of Hammett-plots is that with known σ-values one can predict values of δ for substituents which were not measured.

In order to get information about the excited state of triazenes some experiments were carried out in the presence of oxygen which is known to function as triplet quencher [35]. However, no change was observed in these experiments compared with those carried out in an argon atmosphere. Therefore the triplet excited state was considered to be unlikely. In contrast, experiments in the presence of pyrene, which is known to be an effective singulett quencher, have shown strong effects, e.g. decrease of the quantum yield by a factor of 5 to 10.

UV-spectra taken from selected triazene support the view, that the 1,3-dipole character is favored when the aromatic ring is substituted with electron withdrawing functions such as NO_2 or CN (**T1, T2**), indicated by absorption at high wavelength with high absorption coefficient (Table 4).

6. IR- AND RAMAN SPECTROSCOPY

A combination of IR and Raman spectra was used for the assignment of the N=N frequency. A survey on the position of the N=N signals of different triazenes is given in Table 5 .

For para-substituted triazenes the frequency ν (N^1=N^2) decreases with increasing electron withdrawing character of the substituent. Meanwhile, the frequency of the N^2-N^3 single bond increases, however, to a smaller extent. This behavior is expected for a 1,3 dipolar resonance structure.

Table 4. UV-absorptions of selected triazenes 4-R_1-Ph-N=N-N$(C_2H_5)_2$

Triazene	R_1	λ_1 (nm)	ε_1 ($lmol^{-1}cm^{-1}$)	λ_2 (nm)	ε_2 ($lmol^{-1}cm^{-1}$)	λ_3 (nm)	ε_3 ($lmol^{-1}cm^{-1}$)
T1	NO_2	242	8400	—	—	371	23700
T2	CN	231	9500	—	—	328	22400
T4	Cl	227	10200	289	17900	320	15500
T5	H	227	8400	285	13900	308	13100
T6	CH_3	228	9300	287	14500	316	13400
T7	OCH_3	222	10300	291	15900	328	14000

Ab initio and semiempirical calculations (AM1, PM3, SCAMP [36]) also support the 1,3 dipolar structure of the triazenes: the highest degree of N^1=N^2-double bond character is calculated for $R_1 = OCH_3$ and the lowest for $R_1 = NO_2$, and corresponding with those results the single bond character for N^2-N^3 increases from $R_1 = NO_2$ to $R_1 = OCH_3$.

7. DOPANT INDUCED LASER ABLATION OF PMMA AT 308 NM

Since the early reports in 1982 [39,40] ablative photodecomposition of polymers became a field of intense investigation. Recently promising results have been published for the ablation of PMMA by a 308 nm excimer laser, using diphenyltriazene as dopant [41].

The following figures show undoped PMMA after irradiation with 308 nm excimer laser (fluence F > 6,5 Jcm^{-2}). In this case PMMA is damaged but not structured (Fig. 10). Better results were received by doping of PMMA with triazenes (Fig. 12): the film surface is now clearly structured. For these experiments films were cast from THF solution of PMMA doped with different amounts of 4-NC-Ph-N=N-N$(C_2H_5)_2$ (**T2**) of 200μm thickness. These films were irradiated with a 308 nm excimer laser with a repetition rate of 2 Hz and a pulse length of 30 ns (fluence between 0,5 and 11,2 J cm^{-2}). Results of the ablation experiments performed on two doped PMMA samples of different molar masses are presented in Fig. 11. The triazene (**T2**) concentration was varied between 1 and 2 wt %.

Doubling the triazene concentration roughly halves the limiting etch depth per pulse. Fig.11 shows also a dependence of the etch depth on the molar mass, indicating that the etch depth is always lower for higher molar masses under comparable conditions.

The ablation quality is also a function of the triazene concentration - sharper, higher quality structures are received when higher triazene concentrations are applied (Fig. 12).

Table 5. Effect of the substituents R_1 in 4-R_1-Ph-N=N-N$(C_2H_5)_2$ on the vibrational frequencies of the triazene group in cm^{-1}

		ν (N^1=N^2)		ν (N^2-N^3)	
Compound	R_1	Raman	IR	Raman	IR
T8	$N(CH_3)_2$	1417/1407	1416/1406	1255	1237
T5	H	1414	1414	1252	1239
T7	OCH_3	1408	1407	1253	1245
T6	CH_3	1403	1403	1254	1237
T3	COOH	1397	1401	1252	1239
T2	CN	1386	1384	1260	1243
T1	NO_2	1391	1383	1259	1246

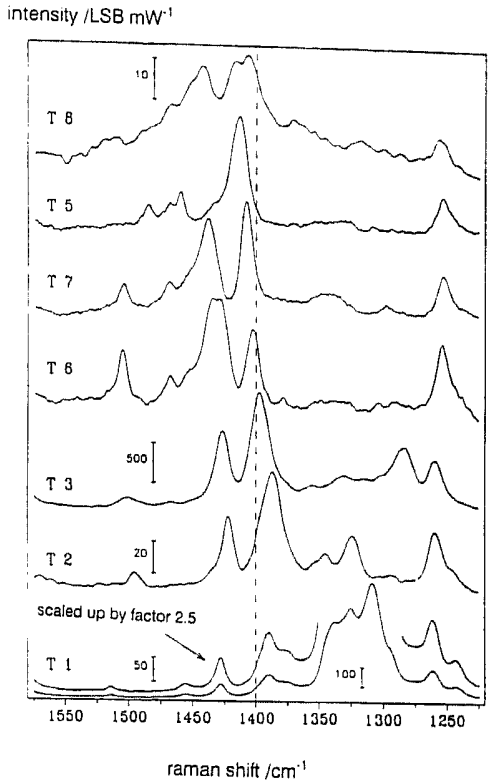

Figure 9. Raman spectra of para-substituted triazenes.

The much better ablation results on the doped material might be best explained on the basis of a "driving gas" effect of the nitrogen formed during irradiation. However, a large quantity of ejected material is seen around the edges of the crater. Furthermore, both the walls and the bottom of the crater exhibit an irregular structure.

These studies demonstrate that non-absorbing polymers can be efficiently doped for 308 nm eximer laser ablation by adding small amounts of substituted 1-phenyl-3,3-dialkyl triazenes. Crater formation is induced by a photochemical ablation mechanism on the basis of photolytic fragmentation of the dopant. Nitrogen acts as driving gas for the ejection of the polymer material. Ablated depth per pulse as high as 80μm have been observed.

The dependence of the etch rate on laser fluence exhibits two regimes, i.e. a linear dependence on the logarithm of fluence $\{\ln (F/F_o)\}$ followed by a plateau region. In the linear

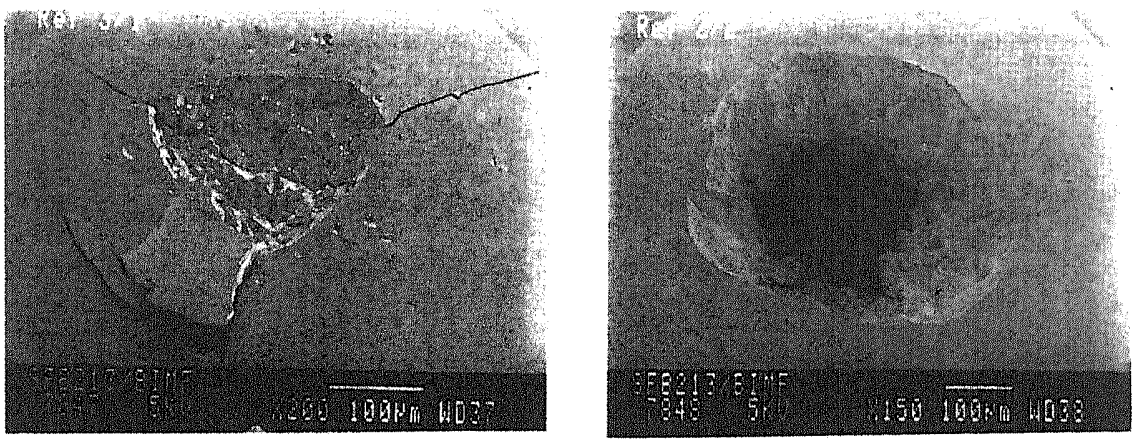

Figure 10. Electron micrograph of PMMA film, irradiated with a 308 nm excimer laser, 1 and 2 pulses (F = 6.5 and 11.7 Jcm^{-2}).

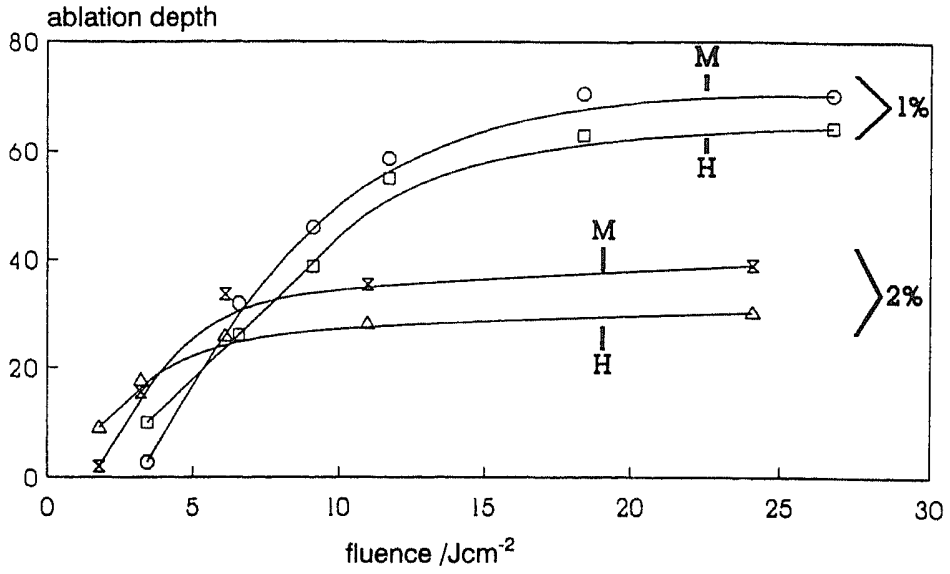

Figure 11. Influence of the molar mass on the ablation characteristics of PMMA doped with 1 and 2 w% of 4-NC-Ph-N=N-N(C_2H_5)$_2$ (**T2**); M = PMMA (M_w = 97000); H = PMMA (M_w = 500 000).

regime, the ablated depth per pulse is proportional to the quantum yield of the photochemical decomposition and follows the 1/c dependence. In the plateau a thermal mechanism, i.e. the absorption of photons followed by the thermolization of the energy, provides the dominant contribution to the ablation. Therefore the photolysis quantum yield QY appears to be no longer of importance.

8. EXCIMER LASER ABLATION OF TRIAZENE POLYMERS

The alternate route to chromophore doped polymers as described above is the tailored synthesis of photopolymers containing a suitable chromophore group, e.g. triazene polymers of the following structure:

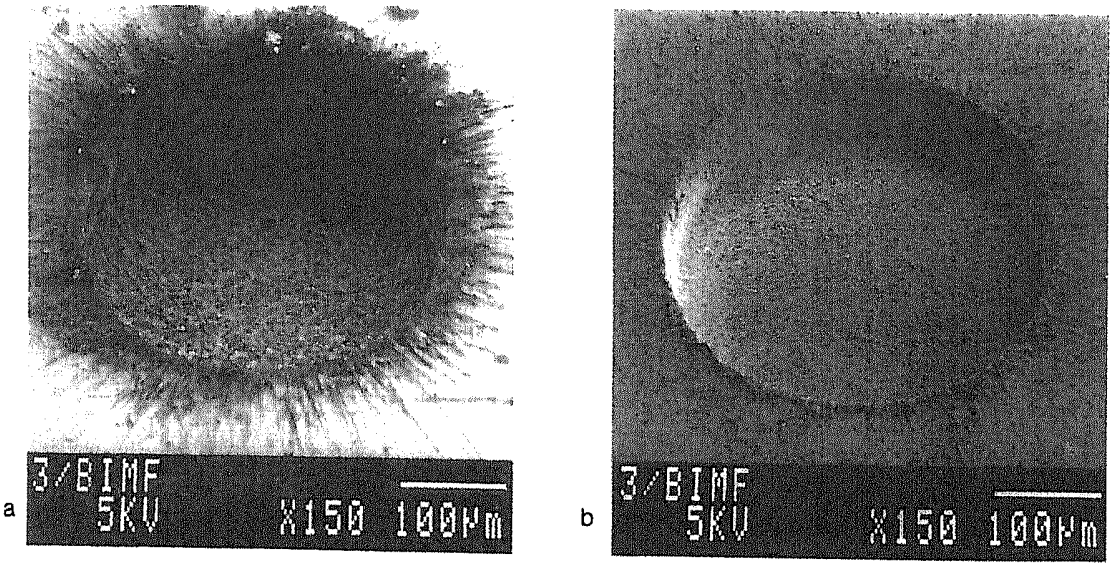

Figure 12. Electron micrograph of laser ablated PMMA doped with **T6**; a) 2mol%, b) 5mol% (F = 5.8 Jcm^{-2}).

Table 6. Structural formulas of investigated triazene polymers

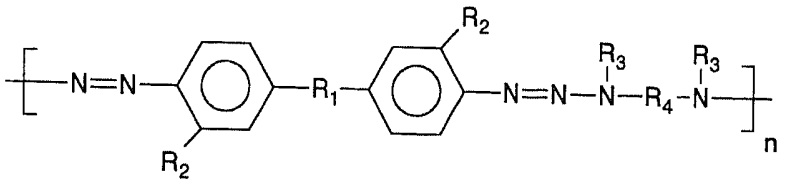

Polymer	R_1	R_2	R_3	R_4
TP1	O	H	CH_3	C_6H_{12}
TP2	O	H	CH_3	C_2H_4
TP3	—	OCH_3	CH_3	C_6H_{12}
TP4	p-SO_2	H	CH_3	C_6H_{12}
TP5	m-SO_2	H	CH_3	C_6H_{12}
TP6	CO	H	CH_3	C_6H_{12}
TP7	O	H	CH_3	C_3H_6
TP8	O	H	C_2H_5	$(CH_2\text{-}CH=)_2$
TP9	CO	H	C_2H_5	$(CH_2\text{-}CH=)_2$

The polymers were synthesized according to the following general procedure: A bis(4-aminophenyl) ether, ketone, or sulfone (R_1 = O, CO, SO_2) was diazotized with the nitrite in hydrochloric acid. The resulting diazonium salt was reacted in situ directly with a substituted α,ω-diaminoalkane to yield the desired product in a polycondensation reaction. The polymers **TP1** through **TP9** were characterized by GPC, NMR spectroscopy, DSC, and TGA.

Molar masses of **TP1** to **TP9** are in the range of 50,000 to 120,000 g/mol (M_w), measured by GPC. From TGA-studies one can conclude that the N_2 and the R_3-N-R_4-N-R_3 unit are released in one step between 210 and 300°C. Some data are summarized in Table 7.

From these polymers films were prepared by casting from THF-solution. After drying films of 100 - 200 μm thickness were received. Technical details about the laser ablation procedure are described elsewhere [41,43].

Polymer **TP8** was chosen as a representative example to illustrate the structures resulting from eximer laser irradiation. A scanning electron micrograph of an ablation crater

Table 7. Physicochemical reference data of triazene polymers

Polymer	M_w ($gmol^{-1}$)	λ_{max} (nm)	ε_1/$lmol^{-1}cm^{-1}$at 308nm (in solution)	photolysis quantum yield (%)
TP1	71,000	330	27,700	0.26
TP2	46,000	353	24,900	0.39
TP3	53,000	367	11,300	0.17
TP4	107,000	336	23,200	0.12
TP5	207,000	293	22,500	0.16
TP6	62,000	352	17,200	0.13
TP7	19,000	331	23,900	0.74
TP8	9,000	334	22,400	0.64
TP9	69,000	357	18,400	0.16

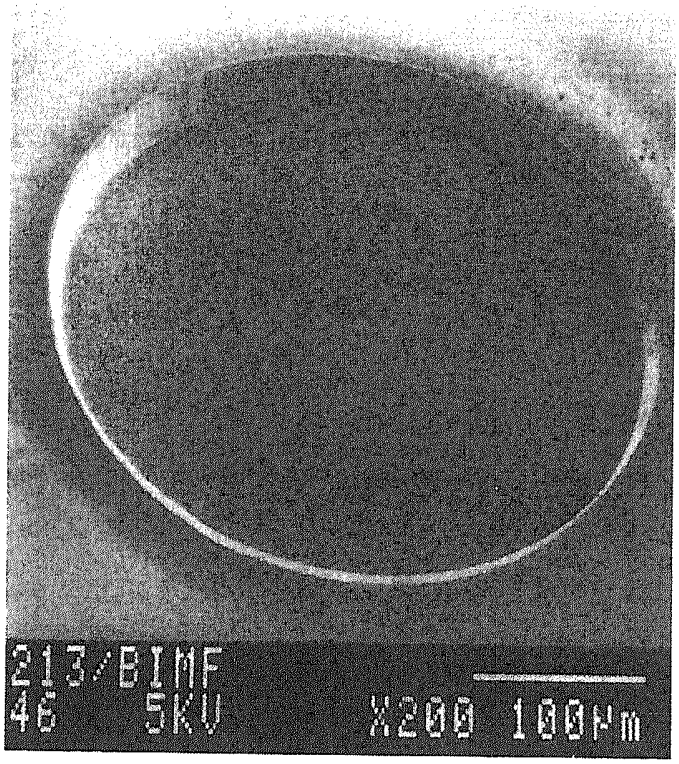

Figure 13. Electron micrograph of **TP8**, irradiated with a 308 nm laser, 100 pulses, fluence = 1.2 J/cm^{-2}.

produced is shown in Fig.13. The sample was irradiated with 100 pulses of 1.2 Jcm^{-2} fluence at 308 nm. Very sharp contours and steep edges were observed for the irradiated area.

Similar sharp contours have been found for all other polymers **TP1** to **TP9**. This favorable behavior which has rarely been observed with any other materials, appears to be an unique property of triazene polymers. For triazene polymers the ablation is fully governed by the photolytic decomposition of the triazene groups.

A striking feature that distinguishes the triazene polymers from other photosensitive materials used in laser ablation is the absence of ejected material deposited around the crater. A possible reason for the absence of solid ablation products, the socalled "debris", is the well-defined fragmentation of the polymers. Small gaseous products, in particular N_2, are acting as a driving gas which promotes at least the initial stages of the ablation.

For all triazene polymers the total ablated depth at given fluence (laser pulse energy per irradiated area) increases linearly with the number of pulses. In the low-pulse energy regime the fluence dependence is well described by the equation:

$$d(F) = \frac{1}{\alpha_{eff}} \ln\left(\frac{F}{F_0}\right) \qquad \text{(E4)}$$

$d(F)$ = ablated depth per pulse
F = laser fluence
F_0 = threshold fluence
α_{eff} = effective absorption coefficients for ablation
(typical data: $\alpha_{eff} = 2 \times 10^4 cm^{-1}$, $F_0 \cong 100$ mJ/cm, $F_0 \times \alpha_{eff} \cong 2$ kJ/cm)

A common feature of the triazene polymers is the absence of any simple relation between the effective absorption coefficients obtained from the ablation data and the molar absorption coefficients at 308 nm in solution. This lack of correlation is not unusual in

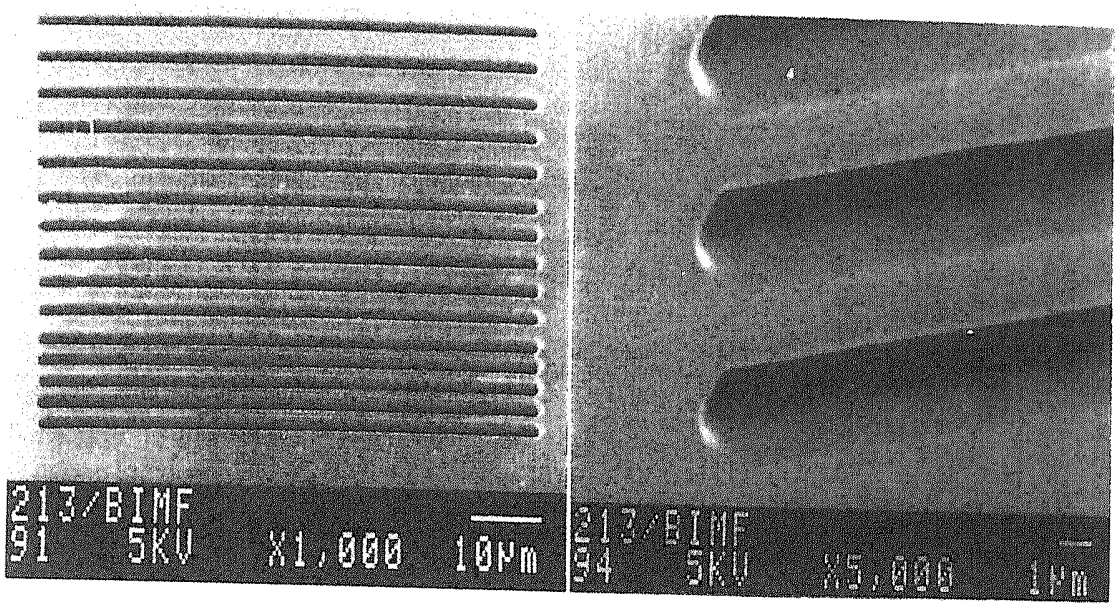

Figure 14. Electron micrograph of laser ablated **TP1** with slit mask applied.

polymer ablation [44] and has been ascribed to nonlinear effects (saturation of absorption, multiphoton effects) and to absorption by laser induced plasma photoproducts [45].

9. RESOLUTION TESTS

The achievable structural resolution by laser ablation was tested for material **TP1**. A rectangular slit mask was imaged onto the sample (coated as described above) to illuminate a stripe of ≈ 1 µm width. The sample was irradiated with 10 pulses of 0.2 Jcm^2 fluence. The results are shown in Fig. 14.

Again, an unique feature is the absence of any solid polymer deposits around developed structures. Furthermore the high resolution tests with the triazene polymers material yield resolutions near to 0.4 µm. These both facts render the triazene polymers very suitable for laser ablation structuring in microlithography.

CONCLUSION

Low molecular triazenes, added to common polymers, and triazene polymers are both suitable for laser ablation. The differences between PMMA doped with low molecular triazenes (A) and polymers containing triazene units in the main chain (B) are as follows:

(A)

- ablation depth ~ 70 µm/pulse
- ablation depth ~ 1/[triazene]
- low level of doping necessary for large effects
- photochemical produced N_2 is driving gas for the ablation
- change from photochemical into photothermical ablation as a function of laser fluence

(B)

- ablation depth ~2-3 µm/pulse

- ablation depth ~ $1/\alpha_{eff}$
- unusual proportionality between photolysis and quantum yield
- sharp contours
- resolution 500A
- no deposits around the ablation crater

REFERENCES

1. P. Griess, Justus Liebigs Ann. Chem. *121*, 258 (1862).
2. A. V. Baeyer, C. Jaeger, Ber. dtsch. Chem. Ges. *8*, 148 (1875).
3. T. Giraldi, T. A. Connors, G. Carter (Ed. s), "Triazenes - Chemical, Biological and Clinical Aspects" Plenum Press, New York, 1990.
4. J. Stebani, PhD Thesis, Bayreuth, 1993.
5. T. Lippert, PhD Thesis, Bayreuth, 1993.
6. F. R. Fronczek, C. Hansch, S. F. Watkins, Acta Cryst. *C 44*, 1651 (1988).
7. M. H. Akhtar, R. S. McDaniel, M. Feser, A. C. Oelschlager, Tetrahedron *24*, 3899 (1968).
8. N. P. Marullo, C. B. Mayfield, E. H. Wagener, J. Am. Chem. Soc. *90*, 510 (1968).
9. L. Lunazzi, G. Cerioni, E. Foresti, D. Macciantelli, J. Chem. Soc.Perkin Trans. II, 686 (1978).
10. O. Nuyken, J.Gerum, R. Steinhausen, Makromol. Chem. *180*, 513 (1979).
11. C. Koningsberger, G. Salomon, J. Polym. Sci. *1*, 200 (1946).
12. US Patent 2.313.233 (1941), B. F. Goodrich Co., Inv. C. F. Fryling, C.A. *37*, 5284^4 (1943).
13. US Patent 2.643.990 (1953), Chemstrand Co., Inv. G. E. Ham, C.A. *47*, 9025i (1953).
14. R. L. Hardie, R. H. Thomson, J. Chem. Soc., 1268 (1958).
15. US Patent 2.376.015 (1945), B. F. Goodrich Co., Inv. W. L. Semon, C. A. *39*, 5545^8 (1945).
16. P. A. Vinogradov, Z. Obsc. Chim. *26*, 2882 (1956).
17. R. H. Smith, B. D. Wladkwski, A. F. Mehl, M. J. Cleveland, E. A. Rudrow, G. M. Chmurny,C. J. Michejda, J. Org. Chem. *54*, 1036 (1989).
18. J. Iley, R. Moreira, E. Rosa, J. Chem. Soc. Perkin Trans. II, 81 (1991).
19. N. J. Isaacs, E, Rannala, J. Chem. Soc. Perkin Trans. II, 899 (1974).
20. O. Pytela, P. Svoboda, M. Vecera, Coll. Czech. Chem. Commun. *46*, 2091 (1981).
21. O. Pytela, T. Nevecna, J. Kavalek, Coll. Czech. Chem. Commun. *55*, 2701 (1990).
22. V. Zverina, J. Divis, M. Remes, M. Matrka, Chem. Prum. *22*, 454 (1972).
23. J. R. Barrio, N. Satyamurthy, H. Ku, M. E. Phelps, J. Chem. Soc., Chem. Commun. 443 (1983).
24. Y. Hashida, H. Endo, K. Matsui, Nihon Kagakku Kaishi *8*, 1433 (1975)
25. J. Baro, D. Dudek, K. Luther, J. Troe, Ber. Bunsenges. Phys. Chem. *87*, 1155, 1161 (1983).
26. M. Julliard, M. Scelles, A. Guillemonat, G. Vernin, J. Metzger, Tetradedron Lett., 375 (1977).
27. M. Julliard, G. Vernin, J. Metzger, Helv. Chim. Acta *63*, 456, 467 (1980).
28. A. Stasko, V. Adamcik, J. Dauth, O. Nuyken, T. Lippert, A. Wokaun, Makromol. Chem. *194*, 3385 (1993).
29. T. Lippert, J. Stebani, O. Nuyken, A. Stasko, A. Wokaun, J. Photochem. Photobiol. A: Chem. *78*, 139 (1994).
30. O. Nuyken, J. Stebani, T. Lippert, A. Wokaun, A. Stasko, Macromol. Chem. Phys. *196* (1995), in print.
31. H. Mauser, Z. Naturforsch. *23b*, 1025 (1968).
32. H. Mauser, V. Starrock, H. J. Niemann, Z. Naturforsch. *27b*, 1354 (1972).
33. H. Mauser, G. Gauglitz, Chem . Ber. *106*, 1985 (1973).
34. J. Polster, Z. Phys. Chem. *NF 97*, 113 (1975).
35. N. J. Turro, Modern Molecular Photochemistry, The Benjamin / Cummings Publ., Menlo, 1978.
36. M. J. S. Dewar, E. V. Zoebisch, E. F. Healy, J. J. P. Stewart, J. Am. Chem. Soc. *107*, 3902 (1985).
37. J. J. P. Stewart, J. Comput. Chem. *10*, 209, 211 (1989).
38. T. Clark, SCAMP 4.30, Universität Erlangen, 1990.
39. Y. Kawamura, K. Toyoda, S. Namba, Appl. Phys. Lett. *40*, 374 (1980)
40. R. Srivivasan, V. Mayne-Banton, Appl. Phys. Lett. *41*, 576 (1982)
41. M. Bolle, K. Luther, J. Troe, J. Ihlemann, H. Gerhardt, Appl. Surf. Sci. *46*, 279 (1990)
42. J. Stebani, O. Nuyken, T. Lippert, A. Wokaun, Makromol. Chem. Rapid Commun. *14*, 365 (1993)
43. T. Lippert, J. Stebani, J. Ihlemann, O. Nuyken, A. Wokaun, J. Phys. Chem. *97*, 12296 (1993)
44. S. Lazare, J. Gramer, Laser Chem. *10*, 25 (1989)
45. S. Lazare, J. Gramer, Chem. Phys. Lett. *168*, 593 (1990)